Estudios Geológicos
julio-diciembre 2023, 79(2), e159
ISSN-L: 0367-0449
https://doi.org/10.3989/egeol.45041.1056

Contribution of Landsat 8 OLI imagery to mapping of lithological series and lineaments: implications for Pb-Zn mineralization exploration in the Boudahar Massif, Eastern High Atlas, Morocco.

Contribución de las imágenes Landsat 8 OLI al mapeo de lineamientos y series litológicas: implicaciones para la exploración de mineralizaciones de Pb-Zn en el macizo de Boudahar, Alto Atlas oriental, Marruecos.

Jaouad Choukrad[1,*], Abdelkhiar Ait Ali[1], Hicham Si Mhamdi[2], Youssef Ouahzizi[1], Nacir El Moutaouakkil[3], Naoufal Saoud[1], Mohammed Charroud[1]

[1] Intelligent Systems, Georessources and Renewable Energy Laboratory, Faculty of Sciences and Technics, Sidi Mohamed Ben Abdellah University, BP 2202, Fez, Morocco https://orcid.org/0000-0001-7303-2781, https://orcid.org/0000-0002-7224-0674, https://orcid.org/0000-0002-0583-2522, https://orcid.org/0000-0002-9574-0495, https://orcid.org/0000-0002-1097-5894

[2] Faculty of Sciences and Technics of Errachidia, Moulay Ismail University, BP: 298, Meknes, Morocco ORCID: https://orcid.org/0000-0002-9008-2059

[3] Geosciences, Water and Environment Laboratory, Faculty of Sciences Rabat, Mohammed V, University of Rabat, BP 1014 RP, Rabat. ORCID: https://orcid.org/0009-0000-6908-6234

*Corresponding author: jaouad.choukrad@usmba.ac.ma

ABSTRACT

The Boudahar massif is located in the southern part of the eastern belt of the Moroccan High Atlas and it corresponds to a reef mass of about ten kilometers in length. Jbel Boudahar is a district of lead-zinc-barite mineralization, known by a strong artisanal exploitation of its ores. This district is characterized by its topography with a contrast of altitude and an arid environment, which makes the information acquired more valuable.

The processing of Landsat 8 OLI data allowed us to extract a lithological and structural map, aiming to make correlations to understand the distribution of lead-zinc mineralization. To this end, several tests were carried out, including the composition of color, principal component analysis and band ratio transformation.

The location of the main deposits at Jbel Boudhar coincides well with the lineament derived from band 1 of principal component analysis and with the dolomitic pliensbachian formations mapped by MNF and BR from Landsat Oli8. A remote sensing geological prospecting model has been established for the Jbel Boudhar lead-zinc deposits, providing a basis for future prospecting of new deposits in a similar context.

Keywords: Boudahar massif; Eastern High Atlas; Landsat 8 OLI image; remote sensing; mapping; lineaments; lithology; lead-zinc mineralization.

Recibido el 25 de abril de 2023; Aceptado el 23 de Agosto de 2023; Publicado online el 8 de Noviembre de 2023

Citation / Cómo citar este artículo: Choukrad J. et al. (2023). Contribution of Landsat 8 OLI imagery to mapping of lithological series and lineaments: implications for Pb-Zn mineralization exploration in the Boudahar Massif, Eastern High Atlas, Morocco. Estudios Geológicos, 79(2), e159. https://doi.org/10.3989/egeol.45041.1056

RESUMEN

El macizo de Boudahar se encuentra en la parte sur del cinturón oriental del Alto Atlas marroquí y corresponde a una masa arrecifal de unos diez kilómetros de longitud. Jbel Boudahar es un distrito de mineralización de plomo-zinc-barita, conocido por una fuerte explotación artesanal de sus minerales. Este distrito se caracteriza por su topografía con contrastes de altitud y ambiente árido, lo que hace más valiosa la información obtenida.

El procesamiento de datos Landsat 8 OLI nos permitió extraer un mapa litológico y estructural, con el objetivo de realizar correlaciones para entender la distribución de la mineralización de plomo-zinc. Para ello se realizaron varias pruebas, entre ellas la composición de color, análisis de componentes principales y transformaciones de ratios de bandas

La ubicación de los depósitos principales en Jbel Boudhar coincide bien con el lineamiento derivado de la banda 1 del análisis de componentes principales y con las formaciones dolomíticas pliensbachienses mapeadas por MNF y BR de Landsat OLI8. Así, se ha establecido un modelo de prospección geológica de detección remota para los depósitos de plomo y zinc de Jbel Boudhar, que proporciona una base para la prospección futura de nuevos depósitos en un contexto similar.

Palabras clave: Macizo de Boudahar; Alto Atlas Oriental; imágenes Landsat 8 OLI; teledetección; mapeo; lineamientos; litología; mineralización de plomo-zinc.

Introduction

The Boudahar Massif corresponds to a large mining district containing a huge reserve of lead, zinc, barite, and calcite, which present an important economic source for local and regional Moroccan citizens. Mineral reserves are exploited in the form of small artisanal mining concessions and surface extraction. The existing geological map does not show the spatial extent of this mineralization and therefore does not explain the direct relations between the hosted rock and the ore bodies (Adil et al., 2004; Choukrad, 2022).

With the development of technology, the use of GIS and remote sensing tools has become an essential investigative step in mining and geological mapping. The objectives of this study are to produce thematic maps such as lineament and lithology maps using Landsat 8 OLI imagery (Choukrad et al., 2020; Es-Sabbar et al., 2020; Si Mhamdi et al., 2017). In fact, these results allow the discovery of several other ore bodies of lead and zinc, which can be developed as future potential mines throughout the Boudahar massif.

Geological Setting

The Eastern High Atlas belt is formed by ENE-WSW oriented ridges corresponding to faulted anticlines with liasic carbonate formations (Choukrad, 2022). These ridges limit the large synclines with marl and limestone deposits dated Dogger and quaternary alluvial deposits (Adil et al., 2004; Choukrad, 2022). The northern boundary of this belt corresponds to the North High Atlasic Fault; however, the South High Atlasic Fault is its southern boundary (Fig. 1A and B). In fact, the Boudahar massif matches the structures linked to the south High Atlas fault; where the Liasic reef massif (Dubar, 1948; Elmi et al., 1999) is oriented ENE-WSW. This massif is a faulted anticline structure (Agard & Du Dresnay, 1965), in which the Jurassic is different from the Paleozoic basement and is made up of E-to-ENE and NNW-SSE faults (Fig. 1C; (Dresnay, 1971; El Kochri, 1996; Adil et al., 2004).

Since 1912, the Boudahar massif has been distinct as a lead, zinc, barite, and calcite district. The mineralization manifests as veins emplaced along E-W to WSW-ENE faults, which are parallel to the elongation of the Boudahar structure. Note that the NW veins are less mineralized and seem to be more frequent in the Liasic reef formations located south of the massif (Agard & Du Dresnay, 1965; Adil et al., 2004).

Methodology and data

Remote Sensing Process

The remote sensing process needs an energy source to illuminate the target; this energy gives off radiation during its pass and interacts with the

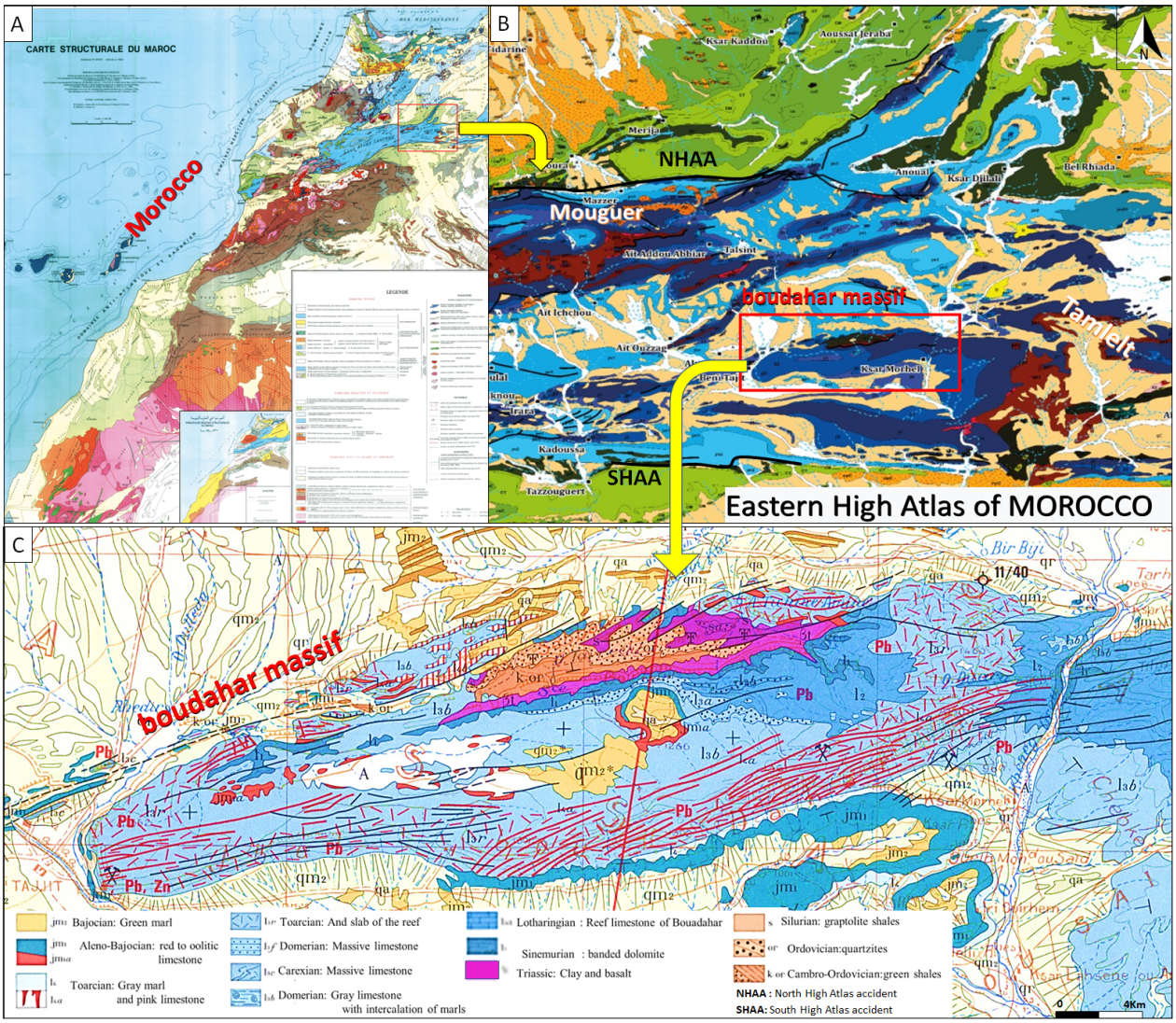

Figure 1.— (A): satellite image of northern Morocco; (B): Eastern High Atlas map (Notes Mem 246. Serv. Géol. Maroc. 1976); (C): geological map of the Boudahar massif (Dresnay, 1971).

atmosphere. A second interaction occurs during the path between the target and the sensor. Once the energy is diffused or emitted by the target, it must be captured remotely (by a sensor that is not in contact with the target) to be finally recorded by the sensor and transmitted, often by electronic means, to a receiving station where the information is transformed into images (Gasmi et al., 2016; Mas, 2000).

A visual and/or digital interpretation of the image after processing is necessary to extract desired information to understand the target and help solve a particular problem.

In this work we used the Landsat OLI 8 image, acquired free of charge from the website. (https://earthexplorer.usgs.gov) on 09/11/2021. This satellite image covers a large part of the structures of the Eastern High Atlas. It is an image formed by 11 bands with different wavelengths and special resolutions (Roy et al., 2014) (Table 1).

As well, we used the geological map of the High Atlas of Anoual-Bou Anane (Eastern High Atlas) at 1/200000 (Michard, 1976) Bni Tajjit at 1/50000 (Notes Mém 601.Serv. Géol. Maroc. 2020)covering the study area to ensure the validation of the acquired

Table 1.— Spectral bands of the Landsat 8 satellite (Roy et al., 2014).

Band number	Description	Wavelength	Resolution
Band 1	Coastal areas / aerosols	0.433 to 0.453 µm	30 meters
Band 2	visible blue	0.450 to 0.515 µm	30 meters
Band 3	visible green	0.525 to 0.600 µm	30 meters
Band 4	visible red	0.630 to 0.680 µm	30 meters
Band 5	Near infrared	0.845 to 0.885 µm	30 meters
Band 6	Short wavelength infrared	1.56 to 1.66 µm	30 meters
Band 7	Short wavelength infrared	2.10 to 2.30 µm	60 meters
Band 8	Panchromatic	0.50 to 0.68 µm	15 meters
Band 9	Cirrus	1.36 to 1.39 µm	30 meters
Band 10	Long wavelength infrared	10.3 to 11.3 µm	100 meters
Band 11	Long wavelength infrared	11.5 to 12.5 µm	100 meters

data by the adopted methodology; where the obtained results are compared with field observations and then validated. Envi, Arc Gis , and RockWorks were used in this satellite image processing study.

Digital Image pre-processing and processing

Before using the satellite image, we carried out a preprocessing which consists of making a radiometric correction followed by an atmospheric correction and finally applying the Dark "Subtraction (DOS)" technique to eliminate the atmospheric noise and the shadow in the image (Adiri et al., 2017, 2020).

"Enhanced" image processing has been applied to clarify geological features. Techniques include color composites (false color RGB), principal component analysis (PCA), spatial filtering, and reporting band.

The major steps of data preprocessing and processing are summarized in the flow diagram below (Fig. 2).

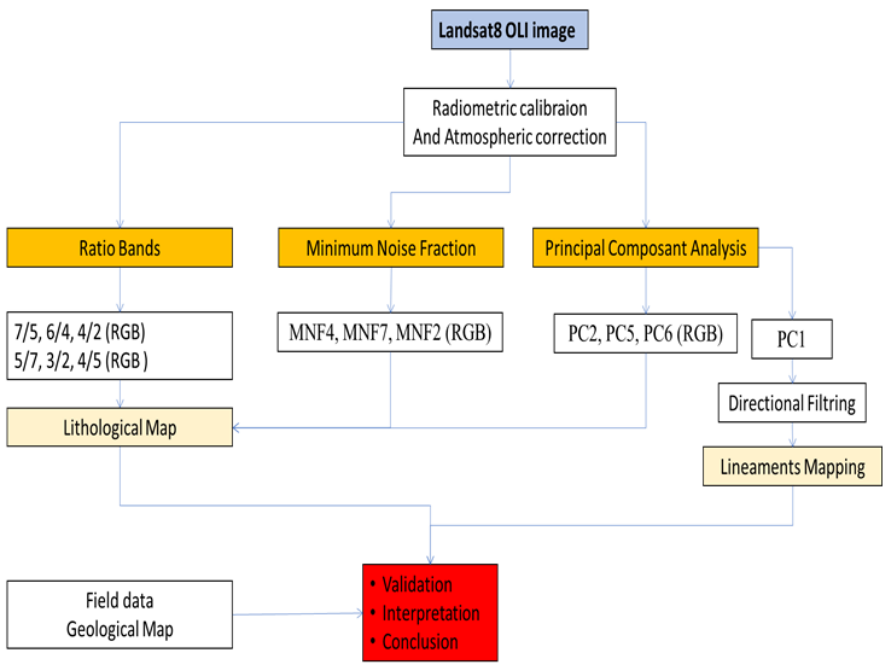

Figure 2.— Flow chart showing the main steps of the methodology approach used.

Band Ratio (BR)

This remote sensing technique is widely used in geological studies and involves a transformation of data by giving the numerical value of one band and dividing it by the numerical value of another band (Mars & Rowan, 2010; Pour & Hashim, 2012). The band ratio is chosen according to the absorption and reflection characteristics of a given target (Pour & Hashim, 2012; Tobi et al., 2022).

MNF

The MNF transform is similar to principal component analysis (PCA) and is used as a preliminary transformation to condense the principal components into a controlled number of spectral bands. The first MNF band contains the signal, and the remaining bands contain the noise. The MNF transformation is applied to all the PIR and IRM bands (VNIR and SWIR) of the ASTER image, and then a combination of colors is used on the result of this transformation.

Principal Component Analysis (PCA)

It's a multivariate statistical method that transforms a set of related variable items into uncorrelated variables. it serves to reduces the number of variables and the redundancy of information (Si Mhamdi et al., 2017). This technique has been applied to geology, cartography and mining studies; it can give good results for the determination of lithological, geological, and structural units(Gasmi et al., 2016; Pour & Hashim, 2012) which will make it possible to link its data with the establishment of mineralization. according to case studies (Adiri et al., 2017; Roy et al., 2014) confirmed that more than 85% of the spectral information is in the early PCA bands.

Lithology Extraction and Mapping

Several ratio combinations have been used in a number of previous works for the purpose of mapping lithological units. These combinations were tested and applied and validated during this study, two combinations were chosen because of their good discrimination of rock units in the study area using the Landsat 8 OLI image (Table 2).

After the preprocessing of the satellite Landsat 8 OLI image, we made several tests of band combinations in RGB on the basis of the spectral signature and the contrasts of the lithological units. Also, the

Table 2.— (A) Parameters values applied for automatic lineaments extraction (Teodoro et al., 2012) (B) Discriminated rock by RGB scale.

A Parametres	**Applied Values**
RADI (Filter raius)	15
GTHR (Edge Gradient Threshold)	55
LTHR (Curve Lenght Threshold)	10
FTHR (Line Fitting Threshold)	4
ATHR (Angular Difference Threshold)	20
DTHR (Linking Distance Threshold)	20

B RGB Scale	**R**	**G**	**B**	**Discriminated rock**	**References**
Ratio Combinations	4/2	6/5	6/7	Iron Oxiedes and clay minerals	(Ali and Pour, 2014)
	5/4	6/5	7/6	alluvium in red color	
	5/6	7/6	4/7	Sandstone and shales respectively	(Adiri et al, 2016)
	5/4	6/5	7/2	alluviom	(Yang et al, 2018)
	5/6	7/6	4/7	Sandston, Liùstone ans shales respectively	
	(4:2)/(6:7)	6/7	4/2	Quartz-rich zone and argilites	(Yousefi et al, 2018)

composite color 257 RGB; PC1-PC4-PC3 (RGB; suggested in this study) was found to be the best method for lithological mapping of the Boudahar massif.

Based on several previous works such as (Choukrad et al., 2020; Tobi et al., 2022), 657 and 257 color composites as RGB images are useful widely in lithologic mapping, they suggest that clay and carbonate minerals are characteristic of absorption of 2.1 to 2.4 µm and reflectance of 1.55 to 1.75 µm. On the same basis, and after visual examination of several RGB band combinations, we found that the 2, 5 and 7 give good discrimination between limestones, sandstones, and alluviums.

The bands (PC2; PC5; PC6) are used for RGB color combinations, which can separate different lithologic facies, this has been verified by field visits and has been confirmed (Fig. 3).

the two images (MNF8 and MNF9) were excluded because the results show that these components did not provide any useful information due to the high level of noise contained in these components. The remaining components are used to produce RGB color composites. The MNF4, MNF7, and MNF2 components are used in RGB. On this image (Fig. 4), most of the lithological units can be identified by simple comparison with the geological map of the area.

Lithology Field Verification

Principal component analysis and band ratio techniques have been evaluated in lithologic mapping.

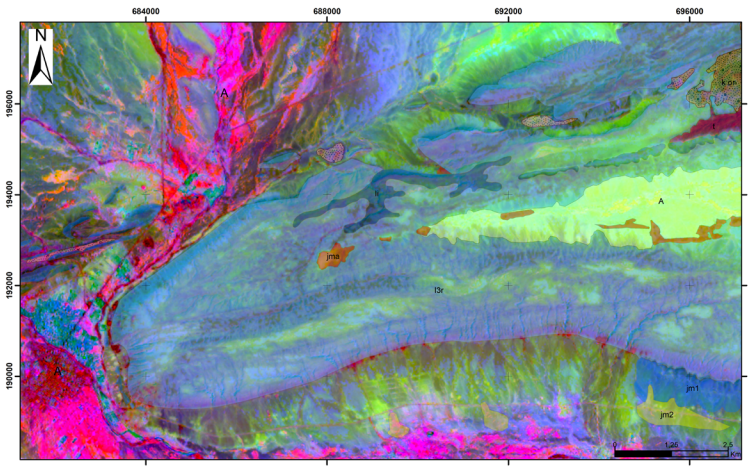

Figure 3.— The PCA technique yielded color composite combinations (PC2, PC5, and PC6 as RGB color).

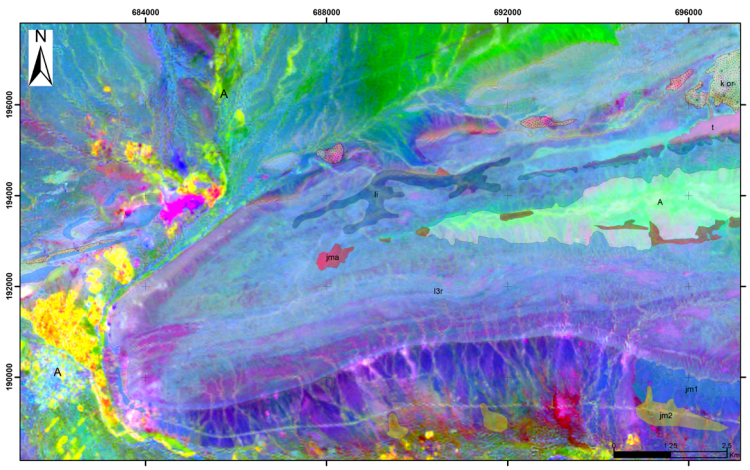

Figure 4.— Color composite combination (MNF 4, MNF 7 and MNF 2 as RGB) obtained from the MNF technique.

In order to have good lithologic outcrop mapping, it is necessary to combine the results of both methods (Fig. 5). The data from the pre-existing map is re-checked by field investigations.

Verification of the acquired maps shows colors that correspond to a series of lithologies that we are trying to find.

Lineaments Extraction and Mapping

Lineaments are defined as structures in lines observed on the Earth's surface and include natural structures of geological and topographical features as well as anthropogenic features (roads, railways, etc.). In order to have a better identification of structural lineaments such as faults, we proceeded to improve the spatial resolution of the OLI image by applying a panchromatic band which has 15m in spatial resolution (Alonso-Contes, 2011). The spectrum bands were resampled at 15 m using the "Pan Sharpening by Gram-Schmid" method (Adiri et al., 2017, 2020; Mahan & Arfania, 2018).

(Es-Sabbar et al., 2020) In this study, we used visual inspection to find the combination of Ratio and RGB (6/5, 7/6, and 4/7) that showed the best ability to identify characteristics. Then, band 6 (SWIR-1) and PC1 are used to obtain the lineaments from the band 6 and PC1 directional filters in different directions. The result is a set of straight lines that are oriented in the main direction of the Boudahar massif and other transverse zones (Fig. 6).

Lineaments field verification

The validation of these results is done with the Google-Earth image (Fig. 7), and by superimposing lineaments on the true color 4-3-2 image or with data collected in the field. We compare it with the elevation map to eliminate any source of noise (peak). To have a better interpretation of the linear structures and their morphologies, the purpose of this step is to remove the linear-curvilinear anthropogenic characteristics of non-geological origin.

Results

Combined Lithological map

The colored composition of a few bands is displayed after processing the satellite image; this method consists of assigning fictitious colors to the spectral bands, allowing the identification of different lithological units. In our case, the best results are obtained with the bands in false colors (7-5-2) to discriminate between the Paleozoic basement facies, the Triassic facies and the Liassic carbonate cover. The band color (7-5-2) and the true color band were compared, and the results were also validated by field missions, in which we checked the compatibility and nature of facies in the Paleozoic basement and in the Mesozoic cover (Fig. 8).

Triassic red clays are rich in mica, and clay and ferrous minerals can be identified by the 7/5 ratio due to

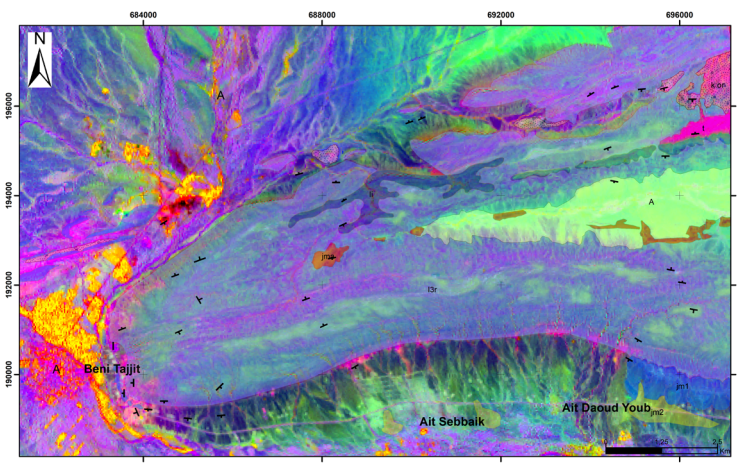

Figure 5.— The band ratio technique yielded a color composite combination (5/7, 3/2, and 4/5 as RGB).

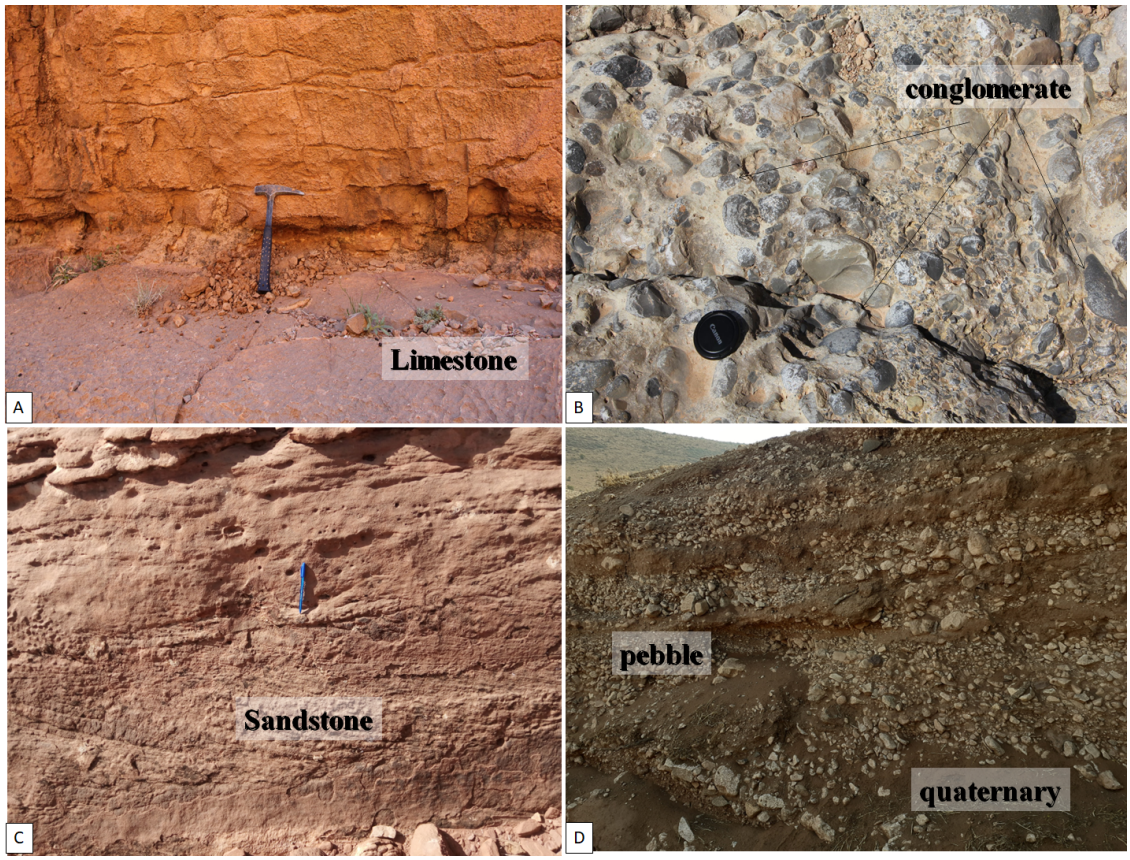

Figure 6.— The main lithological facies of the Boudahar massif, (A): limestones; (B): conglomerates; (C): sandstones; and (D): quaternary deposits

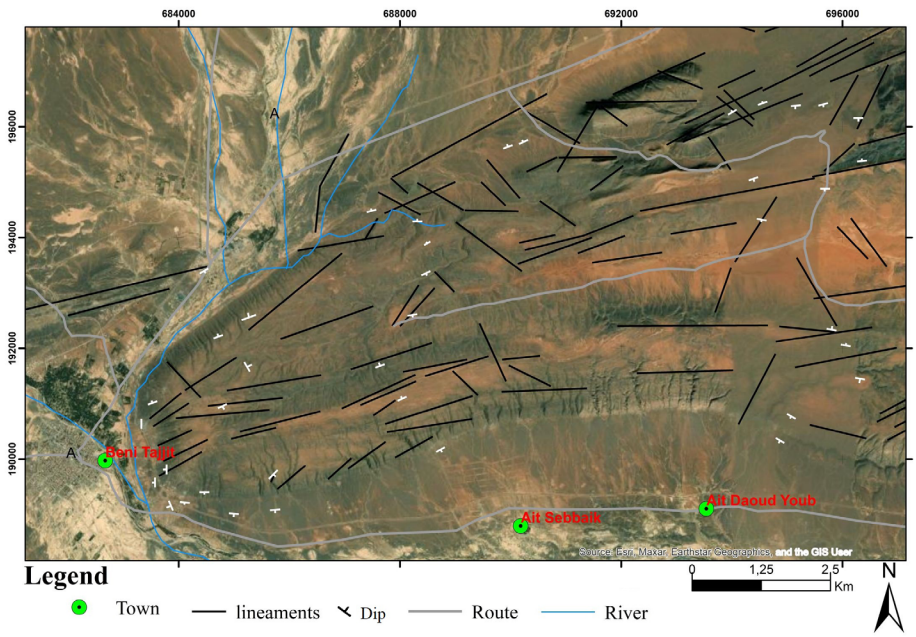

Figure 7.— Band 6 and PC1 directional filters lineament map

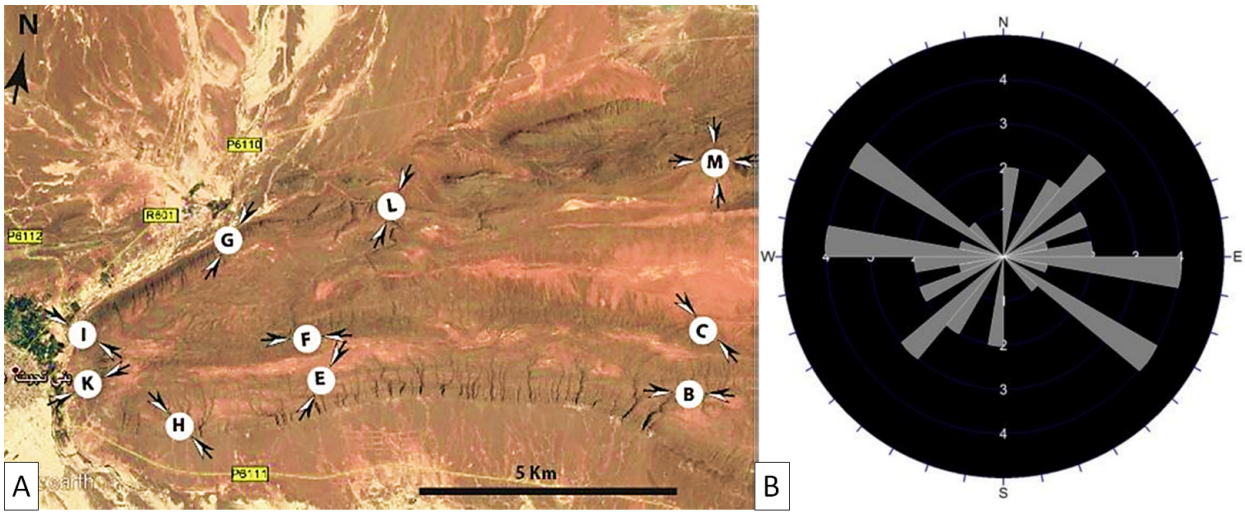

Figure 8.— (A): lineament validation station; (B): validation station directional rosette

its high reflectance in band 7 and absorption in band 5(Harris, 2013). The 3/2 band ratio is also used to identify rocks containing iron oxides (Choukrad et al., 2020; Mahan & Arfania, 2018). Based on these observations, the 4/5 ratio (Fig. 8) shows that limestone has a clear reflection in band 6 and absorption in band 4.

Verification of the results shows that the pink-colored formations are attributed to the basement quartzite and schist, and the yellow to the conglomerate facies. Otherwise, the blue colors in the map correspond to the carbonate formations (Fig. 9).

The PCA gave better results concerning the discrimination of sand and alluvium. Whereas, the combination of band ratios shows better discrimination of limestone and sandstone. The RGB image of band ratios 5/7, 3/2, and 4/5 is blue in color and it mainly covers the center of the studied area, which corresponds to the Liasic reef limestone.

In this work, principal component analysis and band ratio techniques were evaluated in lithologic mapping. In addition, in order to have an exhaustive geological map of the outcrops, we combined the results of these two methods. The result of this comparison shows that the PCA gave better results concerning the discrimination of sand and alluvium. Whereas the combination of the band ratios shows better discrimination of limestone and sandstone.

Combined Lineaments Maps

The compilation of the lineaments resulting from the filtering of the first principal component, band 5 of the colored composition, gave us a synthetic map of the lineaments for the western part of the Boudahar massif (Fig. 10). The analysis of the map shows the dominance of lineaments-oriented E-W to NNE-SSW and the dominance of lineaments that have lengths of between 1000 and 3000m.

Visual interpretation identifies 124 fractures, varying in length from up to four kilometers. The lineament diagram highlights two fault systems, E-W and NE-SW, which are the most represented compared to these oriented NNE-SSW and NW-SE (Fig. 11).

Combined geological and mining map

The study area shows intense fracturing that was identified during fieldwork. Many of these faults are accompanied by brecciated filling with Galena, Calamine, White Calcite, and angular fragments of limestone. This mineralization manifests as veins trending N80 to N90 and some leaded veinlets trending N120 (Fig. 12). The N60 direction is not mineralized; it is filled with calcite and some traces of red clay. Lead-zinc mineralization occurs as decimetrical thick structures and metric to kilometric extents of hosted ore bodies in Middle Liassic limestone formations.

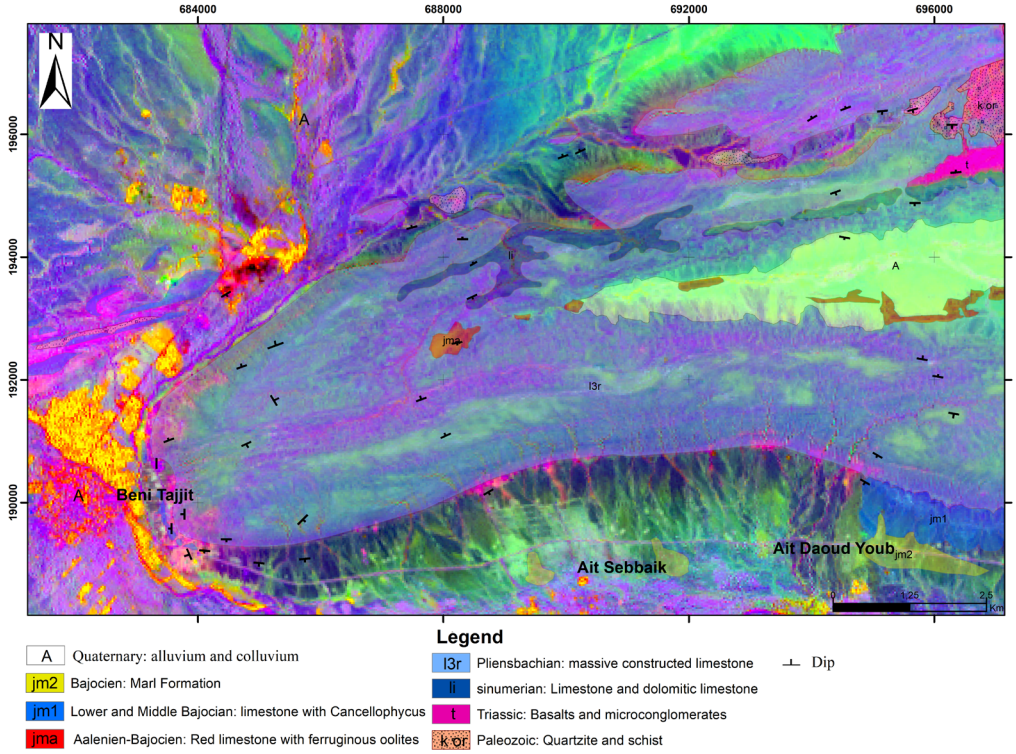

Figure 9.— The band ratio technique yielded a color composite combination (5/7, 3/2, and 4/5 as RGB)

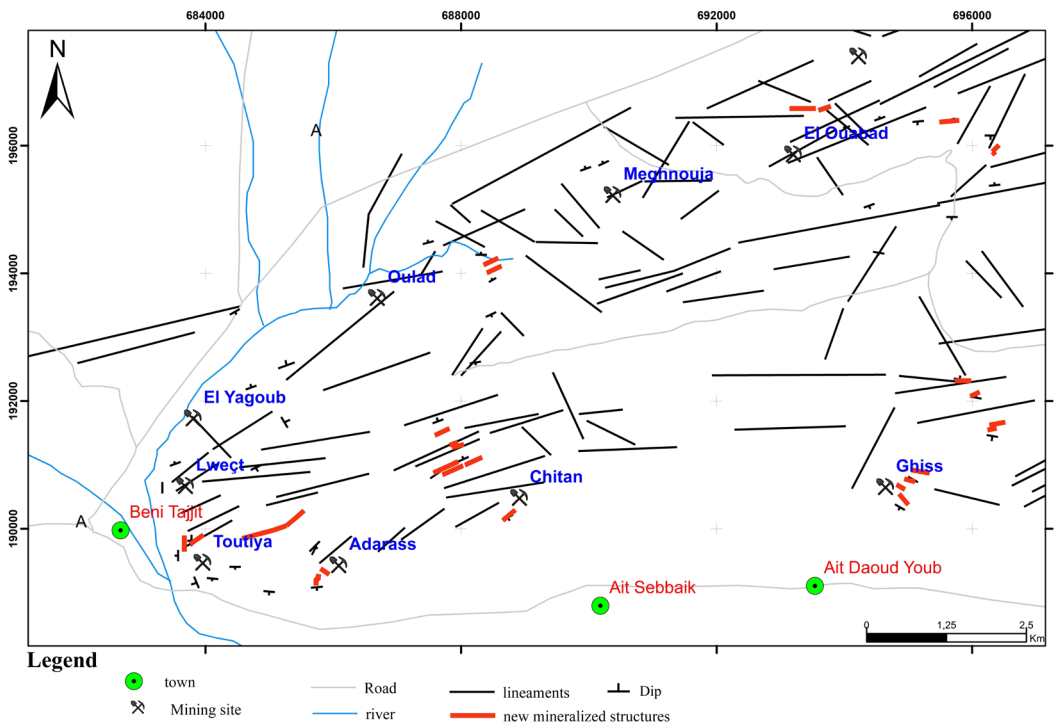

Figure 10.— Synthetic map of the lineaments of the Boudahar massif and distribution of mineralized veins.

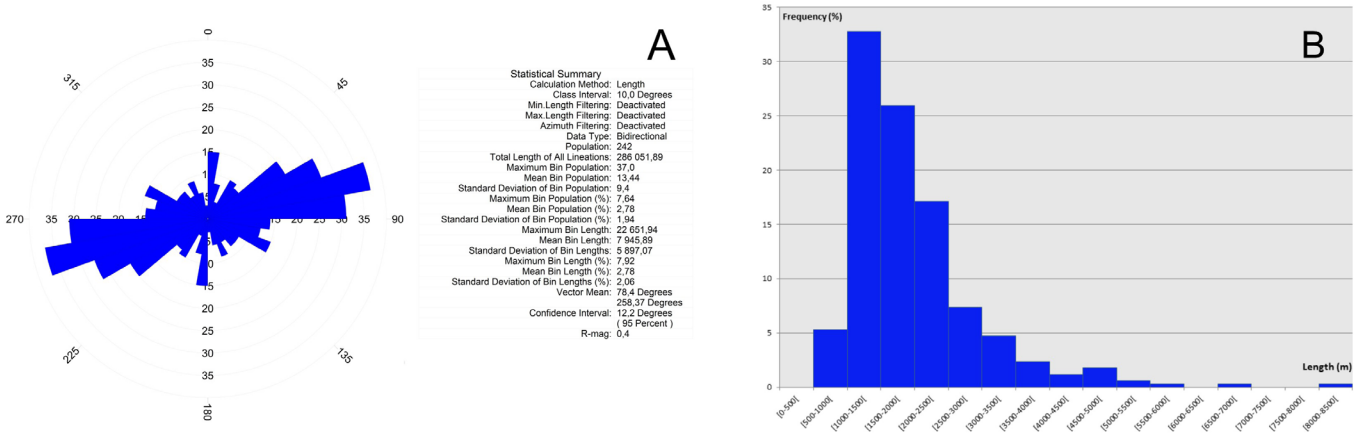

Figure 11.— Diagram of the distribution of orientations (A) and frequency and according to length (B) of the lineaments of the Boudahar massif.

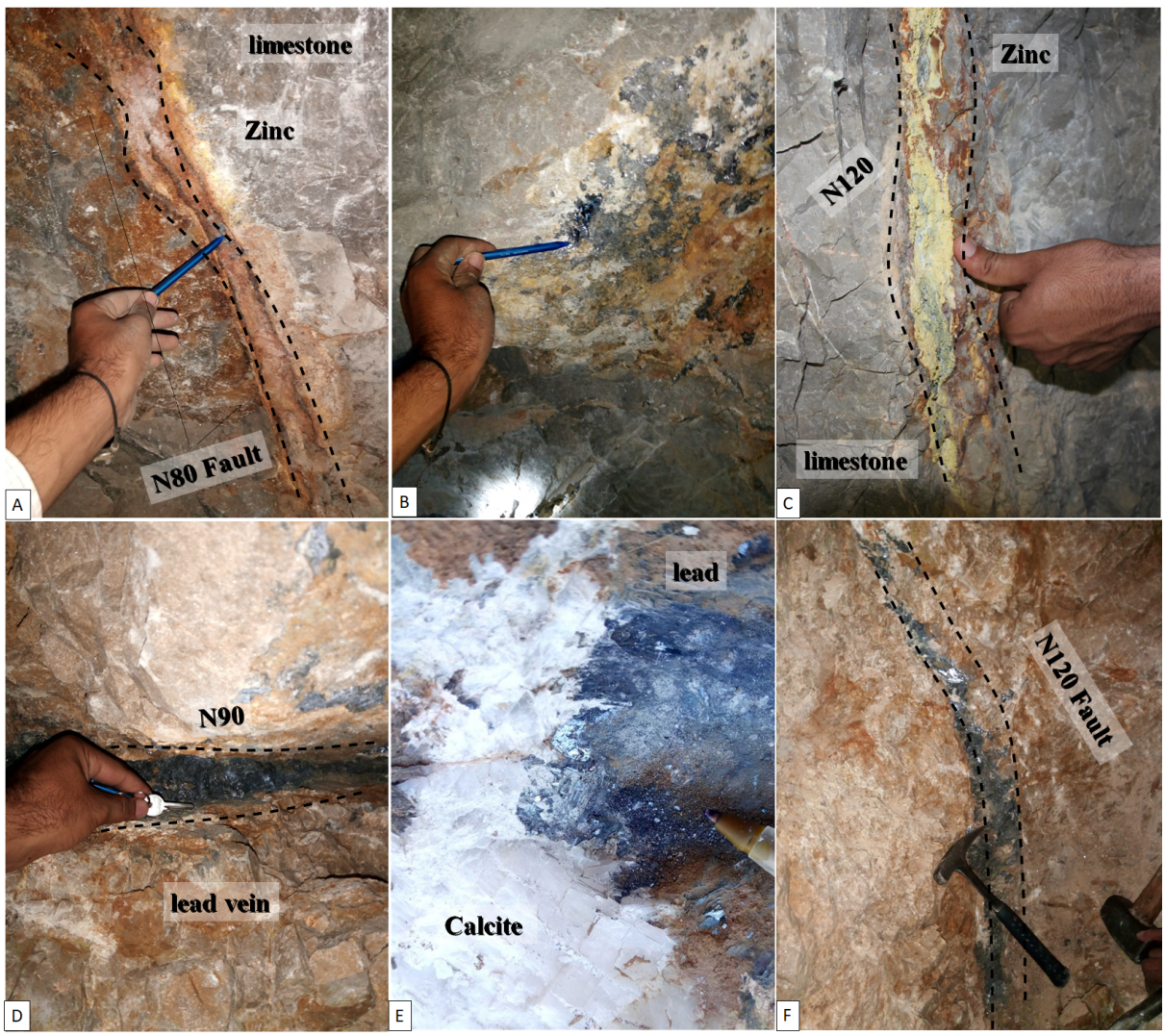

Figure 12.— Artisanal mining trenches (A)-(B); (C): lead-zinc mineralization; (D) and (F): fault-veins directions show different ore fillings with lead veins; and E: calcite and Galena veinlets.

We proceeded to the elaboration of the synthetic geological map of the Boudahar massif from the lithology and lineament maps, as well as combining them with the field data and the previous work concerning the associated mineralization. The result is a map that shows the different geological units of the northeastern part of the Boudahar massif where the Paleozoic quarzitic inlier outcrops are enclosed by Triassic clay and basaltic series, surmounted by the Liassic carbonate series and surrounded by Quaternary alluvium (Fig. 13). The majority of the mineralization is contained in the Liassic carbonate formations, especially along the ENE-WSW faults crossing this Paleozoic massif.

Discussion and Conclusion

The methodological approach used in this work is a set of processed Landsat 8 OLI images of the Boudahar massif. The result is a map of the lithological series and the lineaments that affect them. The combination of the results acquired from these applied techniques and the data collected from the field show the reliability of the mapping and explains the relationships between the type of hosted rock presented as massive and reef limestones of the Middle Lias and the mineralized ore bodies along the fault zone. Processing these techniques allows precision, saving time and allowing easy access to the information on the condition of making good processing choices and also performing field checks.

The production of these maps allowed us to delimit the potential zones of mineralization and to quantify their extent. Indeed, the extracted lineaments are parallel to the ENE-WSW direction, which could sometimes transverse to NW-SE. It is a dense and large vein system; more than 30% of the mapped veins are between 1 and 2 km long and highly mineralized, which allowed them to be classified as a large lead-zinc deposit. These new results push exploration towards new undiscovered fault zones and guide mining exploration and operations in the Boudahar massif.

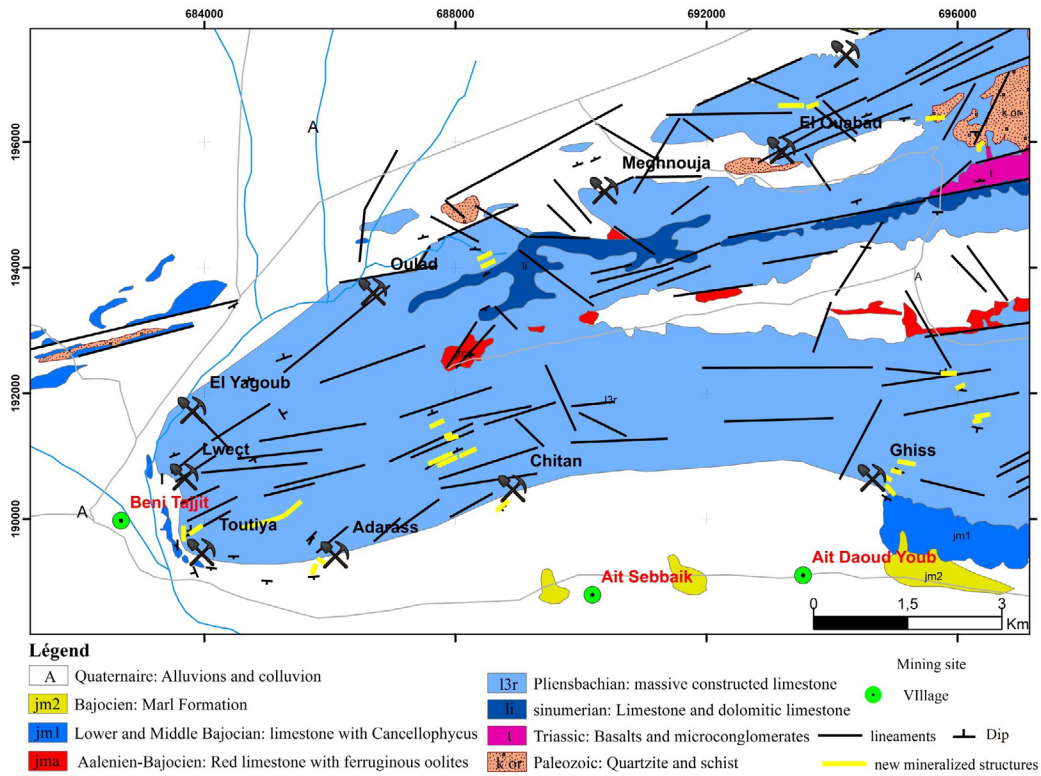

Figure 13.— Synthetic geological map of the mineralized zone of the Boudahar massif.

References

Adil, S., Bouabdellah, M., Grandia, F., Cardellach, E., & Canals, À. (2004). Geochemistry of fluids associated to the Bou-Dahar Pb-Zn Mississippi Valley-type deposits (Morocco). Comptes Rendus-Geoscience, 336(14), 1265-1272. https://doi.org/10.1016/j.crte.2004.06.010

Adiri, Z., El Harti, A., Jellouli, A., Lhissou, R., Maacha, L., Azmi, M., Zouhair, M., & Bachaoui, E. M. (2017). Comparison of Landsat-8, ASTER and Sentinel 1 satellite remote sensing data in automatic lineaments extraction : A case study of Sidi Flah-Bouskour inlier, Moroccan Anti Atlas. Advances in Space Research, 60(11), 2355-2367. https://doi.org/10.1016/j.asr.2017.09.006

Adiri, Z., Lhissou, R., El Harti, A., Jellouli, A., & Chakouri, M. (2020). Recent advances in the use of public domain satellite imagery for mineral exploration : A review of Landsat-8 and Sentinel-2 applications. Ore Geology Reviews, 117, 103332. https://doi.org/10.1016/j.oregeorev.2020.103332

Agard, J., & Du Dresnay, R. (1965). La région minéralisée du Jbel Bou-Dahar, près de Beni Tajjit (Haut Atlas oriental): Étude géologique et métallogénique. Notes et Mémoires du Service Géologique de Maroc, 181, 135-166.

Alonso-Contes, C. A. (2011). Lineament mapping for groundwater exploration using remotely sensed imagery in a karst terrain : Rio Tanama and Rio de Arecibo basins in the northern karst of Puerto Rico [Master Thesis]. Michigan Technological University. https://core.ac.uk/download/pdf/151508664.pdf

Michard A. (1976). Eléments de géologie marocaine. Notes et Mémoires du Service Géologique de Maroc, 252.

Choukrad, J., Elmoussalim, A., Saoud, N., Mounir, S., Assabar, N., Ait Ali, A., & Charroud, M. (2020). Application of remote sensing in the identification and extraction of lineaments and the calculation of mining showings in the Mesozoic cover of the Tazekka massif of Morocco (Maghraoua region). International Journal of Earth Sciences and Engineering, 11(3), 1-8.

Choukrad, J. (2022). Geological context of the establishment of mineralization in the Eastern High Atlas [Doctoral Thesis]. Sidi Mohamed Ben Abdellah University.

Dresnay, R. Du (1971). Extension et developpement des phenomenes recifaux jurassiques dans le domaine atlasique marocain, particulierement au Lias moyen. Bulletin de la Societe Geologique de France, S7-XIII(1–2), 46–56. https://doi.org/10.2113/gssgfbull.s7-xiii.1-2.46

Dubar, G. (1948). Etudes paléontologiques sur le lias du Maroc : La faune domérienne du Jebel Bou-Dahar, près de Béni-Tajjite: Étude suivie de celle de quelques Mollusques d'autres gisements marocains. Notes et Mémoires du Service Géologique, 68.

El Kochri, A. (1996). Géométrie et mécanismes de la déformation du Haut Atlas Centro-oriental (Maroc) [Doctoral Thesis]. Université Mohammed V, Rabat.

Elmi, S., Amhoud, H., Boutakiout, M., & Benshili, K. (1999). Cadre biostratigraphique et environnemental de l'evolution du paleorelief du Jebel Bou Dahar (Haut-Atlas oriental, Maroc) au cours du Jurassique inferieur et moyen. Bulletin de la Société géologique de France, 170(5), 619-628.

Es-Sabbar, B., Essalhi, M., Essalhi, A., & Mhamdi, H. S. (2020). Lithological and Structural Lineament Mapping from Landsat 8 OLI Images in Ras Kammouna Arid Area (Eastern Anti-Atlas, Morocco). Economic and Environmental Geology, 53(4), 425–440. https://doi.org/10.9719/eeg.2020.53.4.425

Gasmi, A., Gomez, C., Zouari, H., Masse, A., & Ducrot, D. (2016). PCA and SVM as geo-computational methods for geological mapping in the southern of Tunisia, using ASTER remote sensing data set. Arabian Journal of Geosciences, 9(20). https://doi.org/10.1007/s12517-016-2791-1

Harris, A. (2013). Thermal remote sensing of active volcanoes: A user's manual. Cambridge university press. https://doi.org/10.1017/CBO9781139029346

Mahan, A., & Arfania, R. (2018). Exploring porphyry copper deposits in the central Iran using remote sensing techniques. Open Journal of Geology, 8(06), 606. https://doi.org/10.4236/ojg.2018.86035

Mars, J. C., & Rowan, L. C. (2010). Spectral assessment of new ASTER SWIR surface reflectance data products for spectroscopic mapping of rocks and minerals. Remote Sensing of Environment, 114(9), 2011-2025. https://doi.org/10.1016/j.rse.2010.04.008

Mas, J. (2000). Une revue des méthodes et des techniques de télédétection du changement. Canadian Journal of Remote Sensing, 26(4), 349-362. https://doi.org/10.1080/07038992.2000.10874785

Pour, A. B., & Hashim, M. (2012). The application of ASTER remote sensing data to porphyry copper and epithermal gold deposits. Ore geology reviews, 44, 1-9. https://doi.org/10.1016/j.oregeorev.2011.09.009

Roy, D. P., Wulder, M. A., Loveland, T. R., Woodcock, C. E., Allen, R. G., Anderson, M. C., Helder, D., Irons, J. R., Johnson, D. M., & Kennedy, R. (2014). Landsat-8 : Science and product vision for terrestrial global change research. Remote sensing of Environment, 145, 154-172. https://doi.org/10.1016/j.rse.2014.02.001

Si Mhamdi, H., Raji, M., Maimouni, S., & Oukassou, M. (2017). Fractures network mapping using remote

sensing in the Paleozoic massif of Tichka (Western High Atlas, Morocco). Arabian Journal of Geosciences, 10, 1-14. https://doi.org/10.1007/s12517-017-2912-5

Teodoro, A. C., Ferreira, D. & Sillero, N. (2012). Performance of commercial and open-source remote sensing/image processing software for land cover/use purposes. 8538, 373-384. https://doi.org/10.1117/12.974577

Tobi, A., Essalhi, M., El Azmi, D., Bouzekraoui, M., & El Ouaragli, B. (2022). Remote sensing and GIS-based mining prospection of Fe-Mn-Pb oxide mineralisation at Jbel Skindis (Eastern High Atlas, Morocco). Estudios Geológicos, 78(2), e147. https://doi.org/10.3989/egeol.44641.614